Practical Time Mark Estimators for Multichannel Digital Silicon Photomultipliers

E. Venialgo, S. Mandai, T. Gong, D. Schaart and E. Charbon

***Abstract*—Multiple time-to-digital converters coupled with silicon photomultipliers allow to timestamp several light photons generated by a scintillation event. Multichannel digital silicon photomultipliers opened the possibility to estimate a gamma-photon time mark by using several photoelectrons timestamps.**

We studied the already-existing statistics models of photoeletron time-stamping generation, while extending the current models by adding the skipping effect. Which accounts for the inability of the system to timestamp a continuous set of photoelectrons.

In addition, we proposed two multiple photoelectron timemark estimators based on the best linear unbiased and the maximum likelihood estimation methods. We calculated the Cramér Rao lower bound for several system parameter and compared it to the proposed estimators' performance. We concluded that under certain system configurations the proposed estimators are efficient.

Moreover, we investigated the effect of the dark count rate on the timing performance. Also, we introduced a filtering method that is based on measuring the time distance between adjacent timestamps. We performed a full Monte Carlo simulation to evaluate the proposed filter efficiency.

Finally, we performed a full Monte Carlo simulation to compare the timemark estimators' performance. We concluded that the best linear unbiased estimator is as efficient as the maximum likelihood estimator. In addition, it was verified that the multichannel digital silicon photomultipliers have a stronger tolerance to dark counts in comparison current digital silicon photomultiplier architectures.

I. Cramér Rao Lower Bound

The Cramér Rao Lower Bound (CRLB) determines a maximum estimation performance for problems that satisfy certain regularity conditions. The CRLB for the particular case of gamma-photon timemmark estimation was analyzed by [1], [2].

In single-photoelectron (q^{th}) timestamp estimation there is only one possible unbiased estimator, which is given by

$$\hat{T_0} = t_q - A, \tag{1}$$

where t_q represents the time-of-registration of the q^{th} photoelectron and A is expressed as

$$A = E[p_q|_{T_0=0}]. \tag{2}$$

The root mean square error (root-MSE) of the single-photoelectron estimation method is equal to the square root of the variance of the PDF (probability density function) of the time-of-registration of the q^{th} photoelectron [2].

$$\sigma_q = \sqrt{MSE(\hat{T_0})}. \tag{3}$$

The maximum timing performance in the single-photoelectron estimation case is determined by Eq. (3). We calculated the performance as a function of the photoelectron order for two different system parameter configurations (see Figs. 1 and 2) called datasets I and II. Dataset I is characterized by 100 ps FWHM jitter and 300 photoelectrons; dataset II by 700 ps FWHM jitter and 3800 photoelectrons. The scintillation decay constants were the same for both cases (LSO with properties [1]). We also calculated the CRLB (intrinsic limit) for each data set [2], [1].

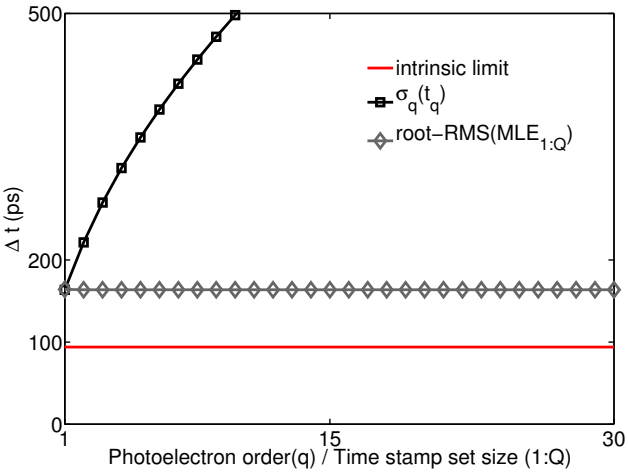

Fig. 1: σ_q and root-CRLB (intrinsic limit) as a function of the photoelectron order for dataset I.

II. Maximum Likelihood Estimation

The likelihood function that corresponds to the $t_{1:Q}$ timestamps of the first Q photoelectrons, when estimating the location parameter (T_0) is defined by

$$L_{1:Q}(t_1, ..., t_Q|T_0) = \frac{R!}{(R-Q)!} \prod_{q=1}^{Q} f(t_q|T_0) \left\{1 - F(t_Q|T_0)\right\}^{R-Q}, \tag{4}$$

where R represents the total number of detected photoelectrons and $f(t)$ represents the pulse shape function convolved with the timing response of the photosensor.

E. Venialgo, S. Mandai, T. Gong, D. Schaart and E. Charbon, are with the TUDelft, The Netherlands, e-mail: E.venialgo@tudelft.nl. The research has received funding from the European Union Seventh Framework Program under Grant Agreement n°289355 (PicoSEC-MCNet). Dennis R. Schaart is supported by the European Union Seventh Framework Program under Grant Agreement n°241711 (SUBLIMA).

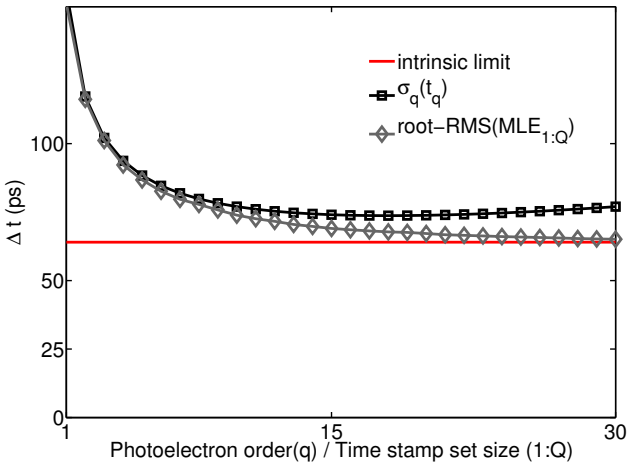

Fig. 2: σ_q and root-CRLB (intrinsic limit) as a function of the photoelectron order for dataset II.

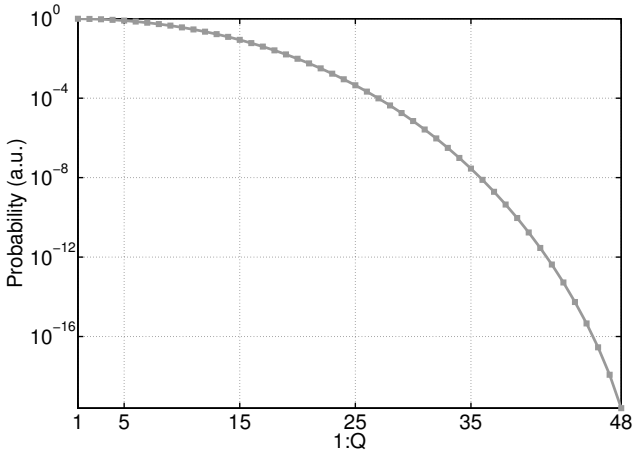

Fig. 3: Probability of measuring a complete set 1:Q without skipping any photoelectron timestamps.

This likelihood corresponds to a type II censored sample of order statistics. The likelihood functions were calculated numerically. We evaluated the performance of this estimator for dataset I and II by utilizing the likelihood functions numerically calculated and a Monte Carlo code (see Figs. 1 and 2) [2].

III. Skipping Effect and Likelihood Function

In the MD-SiPM (multichannel digital silicon photomultiplier) architecture, each TDC (time-to-digital converter) shares 8 or 9 SPAD cells through an OR gate [3]; therefore, when a TDC detects a photoelectron, it becomes unavailable for subsequent detections and the overall detection probability decreases. Therefore, it is not possible to timestamp a continuous set of photoelectrons unless the digital silicon photomultiplier features one TDC per pixel.

If we considered a constant detection probability for every set composed by SPAD cells and a TDC, the decrease in detection probability can be calculated by Eq. (5). We call this decrease in detection probability the skipping effect [2].

$$P(1:Q) = \prod_{i=1}^{Q} \frac{(N_{TDCs} - i + 1)}{N_{TDCs}} \tag{5}$$

Fig. 3 shows the probability of measuring a complete set 1:Q without skipping any photoelectron timestamps.

In addition, the photoelectron timestamp probability distribution that includes the skipping effect can be modeled as a two-stage order-statistics process by assuming constant detection probability [2]. Firstly, we model the time distribution of the unsorted timestamps measured by any TDCs scaling the amount of received photons by a group of a TDC and eight SPAD cells. In addition, we considered that only the first photoelectron is detected (see Eqs. 6 and 7). This time distribution is called $f_{\rm k}(t)$. In order to obtain the likelihood function we replaced in Eq. (4) $f(t)$ by $f_{\rm k}(t)$ and R by the total number of TDCs ($N_{\rm TDCs}$).

$$R' = \frac{R}{N_{\rm TDCs}}, \tag{6}$$

$$f_{\rm k}(t) = R'[1 - F(t)]^{(R'-1)} f(t). \tag{7}$$

IV. MLE and BLUE DCR and Skipping Effect

We performed a final Monte Carlo simulation and compared the performance of two timemark estimators, which were the best linear unbiased estimator (BLUE) and the maximum likelihood estimator (MLE). In addition, we performed simulations for several DCR levels.

The simulated LSO and its properties were according to [1]. The total jitter of the system was 180 ps. The total number of detected photoelectrons was set to 800. We chose a relatively low number of photoelectrons because we assumed that the limiting factor is the total number of SPAD cells, which is 416.

Dark counts were included in this simulation. In addition, a DCR filtering method was implemented to filter out dark counts by measuring the time distance between adjacent registered registered TDCs' events (see Fig. 4). As depicted in Fig. 4, the first three dark counts can be filtered out. Fig. 5 shows the timestamps that were detected as dark counts by the DCR filter under several DCR conditions.

Fig 6 shows the performance of the BLUE and the MLE under several DCR conditions [2]. As observed in the previous figure, MLE and BLUE have almost the same performance. However, BLUE is much simpler in terms of computing power. Subsequently, it can be implemented in real time hardware and achieve a favorable performance.

V. Current Work

In our lab., we have designed a small animal PET detector module composed of 8 small chip-on-boards (see Fig 7). Each chip-on-board contains an array of 9x18 MD-SiPMs. The small chip-on-boards are connected onto a motherboard that contains an FPGA for controlling the MD-SiPMs. This detector is partially manufactured, the motherboard is currently being assembled.

Furthermore, we designed a PCB that contains a small form-factor FPGA to control a single chip-on-board (see Fig. 8).

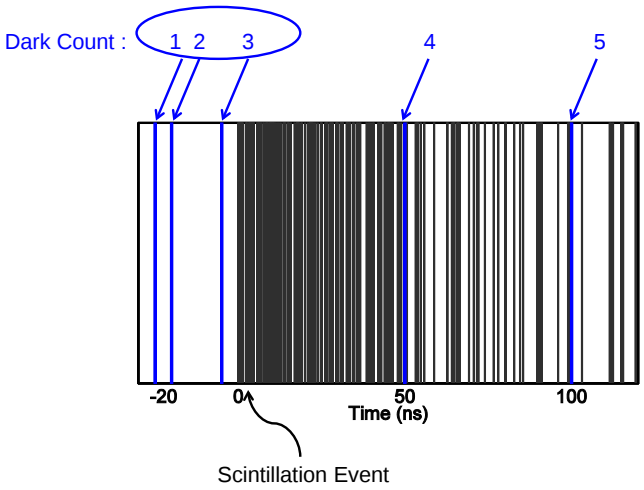

Fig. 4: DCR filter illustration.

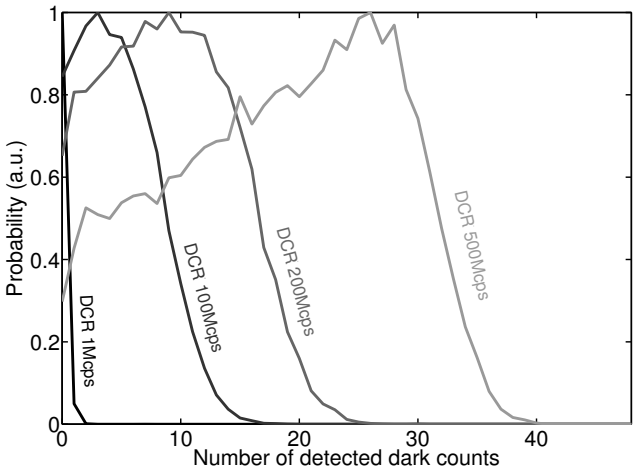

Fig. 5: Detected DCR counts by the DCR filter as a function of the DCR level.

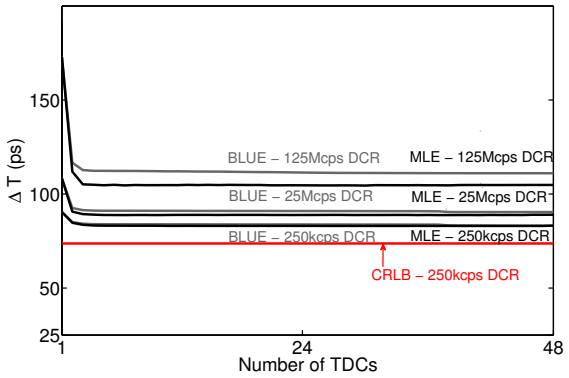

Fig. 6: Single detector root-MSE (ΔT) for several estimators for different DCR levels with contidition I.

The targeted application of this miniaturized PET detector is endoscopic PET. This detector has been manufactured and currently is under testing and characterization.

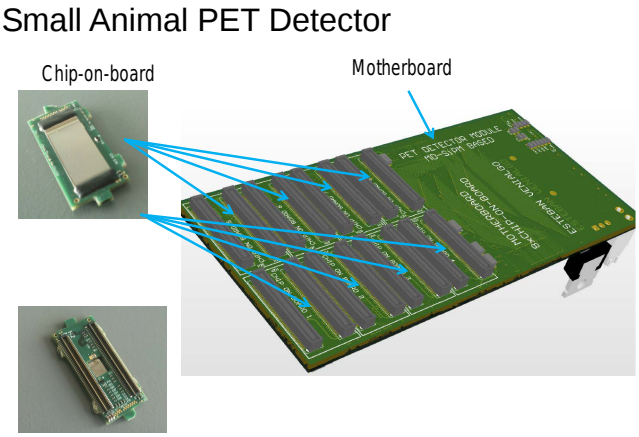

Fig. 7: MD-SiPM Small Animal PET Detector Module.

Endoscopic PET Probe

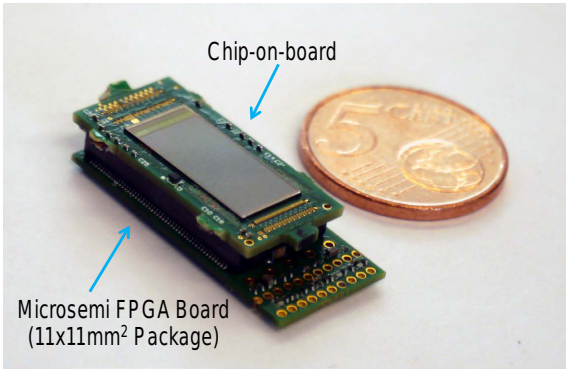

Fig. 8: MD-SiPM Endoscopic PET Detector Module.

References

[1] S. Seifert, H. van Dam, and D. Schaart, "The lower bound on the timing resolution of scintillation detectors," *Phys. Med. Biol.*, vol. 57, no. 7, p. 1797, 2012.

[2] E. Venialgo, S. Mandai, T. Gong, D. R. Schaart, and E. Charbon, "Time estimation with multichannel digital silicon photomultipliers," *Physics in Medicine and Biology*, vol. 60, no. 6, p. 2435, 2015. [Online]. Available: http://stacks.iop.org/0031-9155/60/i=6/a=2435

[3] S. Mandai and E. Charbon, "A 4 x 4 x 416 digital sipm array with 192 tdcs for multiple high-resolution timestamp acquisition," *Journal of Instrumentation*, vol. 8, no. 05, p. P05024, 2013.